Heliyon 10 (2024) e29440

Contents lists available at ScienceDirect

Heliyon

journal homepage: www.cell.com/heliyon

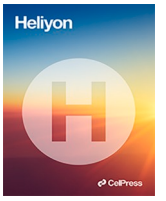

Research article

Green synthesis of yeast cell wall-derived carbon quantum dots with multiple biological activities

Pardis Sadat Mirseyed [a], Sareh Arjmand [a,*], Moones Rahmandoust [a], Shahpour Kheirabadi [c], Rojin Anbarteh [b]

[a] Protein Research Center, Shahid Beheshti University, Tehran, Iran
[b] Antimicrobial Resistance Research Center, Institute of Immunology and Infectious Disease, Iran University of Medical Sciences, Tehran, Iran
[c] Department of Animal Science, College of Agriculture and Natural Resources, University of Tehran, Karaj, Alborz, Iran

ARTICLE INFO

Keywords:
Saccharomyces cerevisiae
Yeast cell wall
Carbon quantum dots
Green synthesis
Hydrothermal

ABSTRACT

Hypothesis: Yeast cell walls are a sustainable biomass source containing carbon and other elements like phosphorus. Converting cell walls into valuable nanomaterials like carbon quantum dots (CQDs) is of interest.
Experiments: Cell walls from *Saccharomyces cerevisiae* were hydrothermally treated in 0.5 M H_2SO_4 to produce CQDs. Multiple analytical techniques were utilized to confirm phosphorus-doping (P-CQDs), characterize the fluorescence properties, determine quantum yield, and evaluate the sensing, antimicrobial, photocatalytic, and antioxidant capacities.
Findings: A successful synthesis of P-CQDs was achieved with strong blue fluorescence under UV excitation, 19 % quantum yield, and excellent stability. The P-CQDs showed sensitive fluorescence quenching in response to ferric ions with a 201 nM detection limit. Antibacterial effects against *Escherichia coli* and *Staphylococcus aureus* were demonstrated. P-CQDs also exhibited dye degradation under sunlight and antioxidant activity. So, the prepared P-CQDs displayed promising multifunctional capabilities for metal ion detection, disinfection, and environmental remediation. Further research is required to fully realize and implement the multifunctional potential of P-CQDs in real-world applications.

1. Introduction

Quantum dots (QDs) are light-emitting nanoscale semiconducting particles that have unusual optical and electronic properties, due to the quantum confinement effect. The dimensions of the QDs are roughly equivalent to those of a large protein (typically in the range of 1–10 nm), made up of 200-10,000 atoms, which is smaller than the exciton Bohr radius of the bulk semiconductor materials. This results in a confinement of the electronic wave function, leading to discrete energy levels and a tunable bandgap that can be controlled by the QDs' size [1,2]. The family of carbon quantum dots (CQDs), including graphene quantum dots, is an emerged and up-and-comer member of the QDs, with distinctive optical, physicochemical, and electrical properties. They are similar in structure and properties to graphene oxide but differ in terms of size [3,4]. Due to their distinct advantages over conventional semiconductor QDs, such as their environmental friendliness, high conductivity, water solubility, low toxicity, and affordable synthesis techniques, these carbon-based nanoparticles have drawn significant attention during the last decade [5,6]. CQDs can also be produced and modified using simple

* Corresponding author.
E-mail address: s_arjmand@sbu.ac.ir (S. Arjmand).

https://doi.org/10.1016/j.heliyon.2024.e29440
Received 2 December 2023; Received in revised form 4 April 2024; Accepted 8 April 2024
Available online 21 April 2024

techniques, making them a promising nanomaterial for a variety of uses, including biosensing, bioimaging, nanomedicine, drug delivery, photocatalysis, photovoltaics, and optoelectronics [7–10].

Pyrolysis, microwave-assisted, and hydrothermal synthesis are the most commonly-used methods used for the fabrication of CQDs from various carbon sources. CQDs can also be doped with various heteroatoms, such as nitrogen, sulfur, boron, and phosphorous, which have been shown to further enhance their properties and expand their potential applications. Different techniques can be used for doping CQDs, including single-step one-pot synthesis, or several-step processes. The choice of doping method can affect the final properties of the CQDs, so the doping procedure must be optimized to produce the desired properties and fully understand the potential of CQDs and their variations [11]. CQDs can be synthesized from any carbon source, ranging from synthetic (different polymers, carbon powder, graphite, etc.) to natural carbon sources (such as leaves, paper, microorganisms, food wastes, plants, etc.) [12,13]. Using cost-effective natural precursors and green fabrication methods for the synthesis of CQDs has been a worthy approach recently, due to considerable cost advantages and environmental waste-management benefits. The CQDs obtained from natural sources roughly possess comparable elemental compositions. However, the presence of non-carbon atoms in the molecular structure of the precursor (such as nitrogen, phosphorous, or sulfur) leads to the synthesis of doped CQDs, with unique properties, without the need for additional surface coating and processing steps [13,14].

The yeast cell wall as a natural carbon resource for the green synthesis of CQDs, due to its high carbon content, is an essential organelle in maintaining the shape and integrity of the organism, and the mechanical strength of the cell, so that it can withstand environmental changes in osmotic pressure [15]. The outer layer of this yeast cell wall mainly consists of mannoproteins, which are negatively charged proteins highly glycosylated with mannose or mannosyl phosphate residues [16,17]; so it contains phosphate, nitrogen, and sulfur atoms. The yeast cell wall is generally produced as a by-product of the yeast extract manufacturing industry. After lysing intact yeast cells, the soluble intracellular fraction (yeast extract) and the insoluble yeast cell wall fraction are separated [18]. Therefore, the utilization of yeast cell walls is very desirable for advantageous waste and cost reduction. The cell wall of *Saccharomyces cerevisiae* species of yeast represents 15–30 % of the cell's dry weight [19] and is mainly composed of glucan (50–55 %), mannoprotein complex (35–40 %), lipid (1–3%), and chitin (1–2%) [16,20], as schematically illustrated in Fig. 1. The composition of yeast cell walls can significantly impact the properties of the synthesized CQDs, including their electronic structure, surface functionalities, and interaction with biological systems. This makes yeast cell walls a multifunctional precursor for CQDs with tailorable properties.

In the present study, the yeast cell wall was extracted from *Saccharomyces cerevisiae* and used as a natural carbon source for the green synthesis of CQDs. The generated CQDs were subsequently analyzed in terms of some physiochemical and biological characterization.

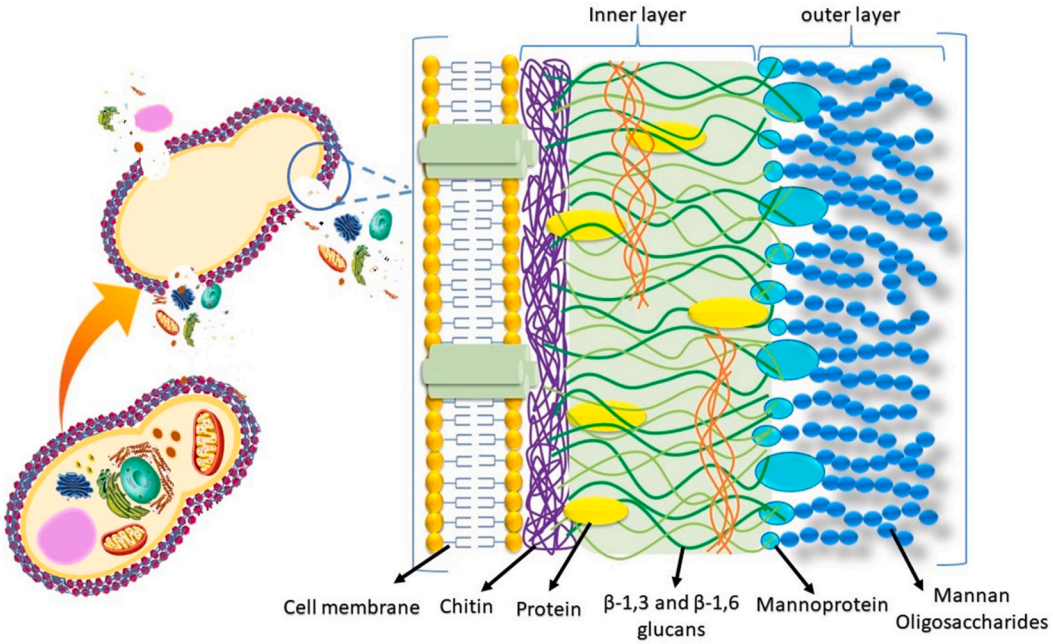

Fig. 1. Schematic illustration of the *Saccharomyces cerevisiae*'s cell wall and the components of its two layers. The inner layer is composed of chitin and β-1,3 and β-1,6 glucan. The mannoproteins and glycoproteins are indicated in the outer layer.

2. Materials & methods

2.1. Yeast cell wall preparation

To isolate the yeast cell wall, enzymatic hydrolysis was employed to lyse the yeast cells, utilizing a protocol previously established in our laboratory. For that, 15 % (w/v) of the baker's yeast cell suspension was prepared in distilled water. After adjusting the pH to 7.0, the suspension was transferred to a glass vessel. A mixture containing equal aliquots of two enzymes, alcalase and flavourzyme (Novozymes), was added at 0.5 % (v/v) concentration and the hydrolysis process was run for 48 h at 55 °C under shaking. After hydrolysis of the yeast, the vessel was boiled for 5 min at 100 °C to terminate the enzymes' activity. The yeast cells before and after hydrolysis were stained with 0.1 % methylene blue solution and observed under light microscopy. The insoluble cell wall was separated from the soluble yeast extract by centrifugation (5000 g for 15 min), and used as the precursor for CQDs synthesis.

2.2. Synthesis of CQDs and calculation of quantum yield

Thermal gravimetric analysis/direct thermal analysis (TGA/DTA) was performed using a TGA-DTA-DSC (SDT Q600-TA Instruments, Spain) to inspect the thermal behavior of yeast cell wall, with the purpose of finding the optimal temperature ranges for CQDs synthesis. Samples of about 20 mg were heated up in helium from 0 to 700 °C with a flow rate of 40 ml/min and a heating rate of 10 °C/min.

A hydrothermal process was applied to generate CQDs from the yeast cell wall. For this reason, a solution of 3 % (w/v) of the yeast cell wall in 0.5 M phosphoric acid was prepared and stirred for 2 h at room temperature. The homogenous solution was transferred to a hydrothermal reactor and placed in an oven at 250 °C for 5 h. The resultant CQDs solution was centrifuged at 7000 g for 30 min, and the supernatant was used for further analysis.

The fluorescent quantum yield (Φ) of the synthesized CQDs was determined using the comparative method with quinine sulfate in 0.1 M H2SO4 as a standard reference. Quinine sulfate has a known quantum yield of 54 % under 360 nm excitation [21] and was prepared in five concentrations in 0.1 M H2SO4 (refractive index (η) 1.63). The CQDs were also prepared in five concentrations dissolved in water (η 1.33). The absorbance of all solutions was kept below 0.1 to minimize reabsorption effects. The fluorescence emission spectra of the CQDs and quinine sulfate dilutions were recorded at 360 nm excitation and the integrated fluorescence intensity was plotted against the absorbance at 360 nm. The gradients of the linear fit for the CQDs (mCQDs) and quinine sulfate (mST) were used to calculate the quantum yield of the CQDs using the following equation:

$$\Phi_{CQDs} = \Phi_{ST}(m_{CQDs} / m_{ST})(\eta_{CQDs} / \eta_{ST})$$

Where ΦST is the known quantum yield of quinine sulfate (54 %), mCQDs and mST are the gradients from the fluorescence intensity plots, and ηCQDs and ηST are the refractive indices of water (1.33) and 0.1 M H2SO4 (1.63), respectively.

2.3. pH, concentration, and storage condition optimization

The pH, storage temperature, and concentration of the obtained supernatant were optimized to achieve a CQDs solution with the maximum fluorescence emission. The pH of the supernatant solution was 1.28 and was adjusted to 3, 4, 5, 6, and 7 using NaOH 1 M. The prepared samples were dropped on Whatman paper, and the fluorescence intensity was visualized under UV light in a Gel-Doc apparatus. The 3 % solution (with optimized pH) was serially diluted to the final concentrations from 1/10 to 1/200. The diluted solutions were stored at 25, 4, and −20 °C for 48 h. The highest detected fluorescence intensity on the Whatman paper was considered the optimized concentration and storage condition. The fluorescence intensities were compared using ImageJ software. Eventually, the optimized CQDs solution underwent dialyzed using a membrane with a 3.5 kDa molecular weight cut off in deionized H_2O, lyophilized, and ground for further analysis.

2.4. Chemical characterization of synthesized CQDs

2.4.1. Optical characterization; UV–visible, fluorescence spectroscopy

The UV–visible absorption spectra of the synthesized CQDs solution were analyzed in the wavelength range of 190–800 nm using a UV/Visible spectrometer (Thermo/Biomate 5 from USA). CQDs were excited at seven wavelengths (310–370) and the corresponding emission spectra (at 350–700 nm) of the CQDs were recorded by a fluorescence spectrophotometer (Thermo, Biomate 5, USA).

2.4.2. Compositional characterization

The set of analytical techniques employed enabled comprehensive characterization of the functionalization, crystallinity, elemental makeup, and doping levels of the P-CQDs synthesized from yeast cell walls.

FTIR analysis was performed using a Frontier FTIR spectrometer (Nexus 470, USA) over the range of 4000-400 cm^{-1} to identify functional groups and chemical bonds present in the yeast cell wall substrate and synthesized P-CQDs. Changes in spectral peaks after CQDs synthesis provide insights into surface functionalization and passivation. The crystalline nature of P-CQDs was analyzed by X-ray diffraction (XRD) using an analytical diffractometer (Philips/PW1730, Poland). Scans were obtained from 2θ angles of 20°–100° at a scan rate of 2 min^{-1}. The diffractograms were indexed to identify crystalline phases based on peak positions and intensities. X-ray

spectroscopy mapping (EDX-MAP) was done using a MIRA II instrument (France) to elucidate the elemental composition and distribution in the cell wall and P-CQDs. This verifies the presence of expected elements like carbon, phosphorus, and oxygen after synthesis. The carbon, hydrogen, nitrogen, and sulfur content of the P-CQDs was quantified using a TruSpec CHNS analyzer (TruSpec/USA) to determine bulk elemental composition.

2.5. Morphological characterization

To prepare P-CQDs for morphological analysis, an ultrasonic treatment was performed to disperse the P-CQDs and prevent aggregation. The zeta potential and particle size analyzer (Horiba Instrument/SZ100, Japan) was used to measure both the size and surface electric charge of synthesized P-CQDs, based on phase analysis light scattering technology. The particle size distribution and electric charge of the P-CQDs in an aqueous solution were obtained from dynamic light scattering (DLS) performed in the automatic mode, using a diode-pumped doubled laser 2 nm light source, with a maximum intensity of 10 mW and wavelength of 532 nm. To minimize the scattering effects, the sample was diluted at a ratio of 1:100 before DLS analysis. Qualitative and quantitative analyses of P-CQDs were performed using transmission electron microscopy (TEM) (CM120/Netherlands). 100 mg of P-CQDs powder was sonicated at 750 W for 5 min and after homogenization, a thin layer of the sample was prepared. The maximum magnification was 180 thousand times and the maximum voltage was 100 kV.

2.6. Fluorescence quenching assay with different salts and in real samples

To evaluate the feasibility of P-CQDs as a fluorescent probe of heavy metals, we used some salts of ions including magnesium sulfate ($MgSO_4$), manganese II chloride ($MnCl_2$), Zinc chloride ($ZnCl_2$), sodium chloride (NaCl), Iron II sulfate ($FeSO_4$) and Iron III chloride ($FeCl_3$). The mixtures containing 0.06 % P-CQDs and 0.5 mM of each salt were prepared and incubated for 5 min at room temperature. The changes in fluorescence intensities and sediment formation were detected using fluorescence measurement. The relative fluorescence intensity (RFI) was used for the calculation of quenching efficiency, which is a measure of the fluorescence signal of a sample relative to a reference or control measurement. It is calculated using the formula:

$$RFI = (F_0 - F) / F_0$$

where F_0 and F represent the steady-state fluorescence intensities in the absence and presence of a quencher or inhibitor, respectively. The salts with P-CQDs quenching ability were analyzed further with increasing concentrations ranging from 10 to 500 μM. The standard curve was plotted and the limit of detection (LOD) and limit of quantification (LOQ) were calculated using the following equations:

$$LOD = 3.3 \times \sigma/S \text{ and } LOQ = 10 \times \sigma/S$$

where σ is the standard deviation of y-intercepts the regression line and S is the slope of the standard curve.

The biosensing potential of synthesized P-CQDs for analyzing Fe^{3+} in complicated biological samples was evaluated in the human serum, using the previously described method [22] and with slight modifications. In brief, the serum sample was allowed to clot by leaving it undisturbed at room temperature for 30 min and then centrifuged at 1500 g for 15 min. The supernatant (the liquid portion of the serum) was separated and diluted 10-fold with Tris-HCl buffer (10 mM, pH = 7.0). Thus, 50 μL of P-CQDs (0.6 mg/ml) and 50 μL different concentrations of Fe^{3+} (0.1–1 μM) were distributed in 400 μL diluted human serum, and incubated for 30 min at room temperature. The fluorescence emission spectra were analyzed at 360 nm excitation wavelength.

2.7. Antimicrobial activity

The antibacterial activity of P-CQDs was determined against a strain of gram-negative *Escherichia coli* (ATCC 25922), and a strain of gram-positive *Staphylococcus aureus* (ATCC 25923) using agar well diffusion and macro dilution methods. In the agar well diffusion assay, the working strains of bacteria were prepared from the frozen strains (−80 °C) by spreading them on the culture plates. Three well-isolated colonies with the same morphological type were transferred into a tube containing 5 ml of suitable fresh medium and incubated at 37 °C until it reached or exceeded the turbidity of 0.5 McFarland (1.5×10^8 CFU/ml). Then, 10^6 CFU/ml of bacteria were cultivated on the Muller Hinton Agar (MHA) plates under aseptic conditions. The 6 mm diameter wells were cut into the surface of the agar using a sterile Pasteur pipette. 100 μl of different dilutions from 3 % (w/v) P-CQDs (in physiology serum) were added to each well and incubated at 37 °C for 24 h. After the incubation period, the diameters of the inhibition zones were measured. Distilled water was used as the negative control and each assay was carried out in triplicate.

The minimum inhibitory concentration (MIC) and minimum bactericidal concentration (MBC) were determined using the Macrodilution method [23]. Twelve two ml serial two-fold dilutions of P-CQDs (started from 3 % (w/v)) were prepared using an autoclaved MHB culture medium. One ml of adjusted bacterial concentration (10^5 CFU/ml) was used to determine MIC. The solution contains only inoculated bacteria in MHB without P-CQDs and the solution contains only P-CQDs without bacteria, considered as negative and positive controls, respectively. The cultures were incubated for 24 h at 37 °C. The lowest concentration of P-CQDs, where no visible growth was detected, was considered as MIC endpoint. 100 μl of cultures with no visible growth were cultivated on the MHA plates and incubated for 24 h at 37 °C. The lowest concentration of P-CQDs that killed 99.9 % of bacteria was considered the MBC endpoint.

2.8. Photocatalytic experiment

The photocatalytic activity of P-CQDs was gauged by the photodegradation of methylene blue aqueous under natural sunlight. A 0.2 % (w/v) mixture of P-CQDs in methylene blue solution (6 mg/ml in distilled water) was prepared and homogenized by magnetically stirring for 1 h at room temperature and in dark. The solution was aliquoted in test tubes (10 ml in each). The tubes were exposed to direct sunlight (~daily temperature = 20 ± 2 °C) for 200 min and during this period 1 ml of solution was collected every 20 min. In the end, the collected samples were centrifuged at 5000 rpm for 10 min to remove the catalyst. The photodegradation of methylene blue was determined based on adsorption at 662 nm using UV/Vis spectrophotometer, which was converted to the methylene blue concentration using the standard calibration curve [24].

2.9. Antioxidant activity

The total antioxidant capacity (TAC) of P-CQDs was determined using a ferric-reducing antioxidant power (FRAP) assay using a commercial standard kit (Naxifer™, Navand Salamat). The FRAP measures the antioxidant power of P-CQDs based on the reduction of colorless ferric-tripyridyltriazine (Fe^{3+}-TPTZ) to an intense blue-colored ferrous-tripyridyltriazine complex (Fe^{2+}-TPTZ) which is measured at 593 nm. The chemistry behind the method was described in detail by Huang et al. [25]. The antioxidant activity was expressed as mmol Fe^{2+} per mg of sample. The experiment was done in triplicate. Trolox, a water-soluble vitamin E analog, was provided by the kit as an antioxidant standard.

3. Results

3.1. Prepared yeast cell walls and P-CQDs

Staining of yeast cells before and after hydrolysis indicated that the cells were completely broken and the content of the cells inside has been removed from the cell wall (Fig. 2a, b). The lysed cell walls were separated using centrifugation and used for further tests.

According to the TGA/DTA analysis of the yeast cell wall (Fig. 3), the phase transformation and weight loss occur around 248.33 °C, implying the thermal decomposition of the yeast cell wall initiated at this temperature. A preliminary analysis of the optical characterization of the generated CQDs was used to determine the heating time. In this work, the hydrothermal treatment of yeast cell wall was performed at 250 °C for 5 h. During synthesis, the sample liquid color turns dark brown and emits fluorescence under UV-light irradiation.

3.2. Condition optimization and quantum yield

Visually, the point on the Whatman paper corresponding to pH 4 had the most fluorescence brightness. Fluorescence intensity quantification using ImageJ confirmed the visual observation (Fig. 4a). The optimality of pH 4 was also verified in PL analysis (section 3.3.1). Diluting the P-CQDs solution up to 1:100 (in the optimized pH) positively affects the fluorescence intensity (Fig. 4b). The temperature of 4 °C (in the optimized pH) showed the highest fluorescence intensity and was chosen as the optimized temperature for the storage of synthesized P-CQDs (Fig. 4c). The quantum yield of synthesized P-CQDs at the optimized conditions was measured to be 19 % using quinine sulfate as the reference. The fluorescent plot of quinine sulfate and P-CQDs are shown in Fig. S1.

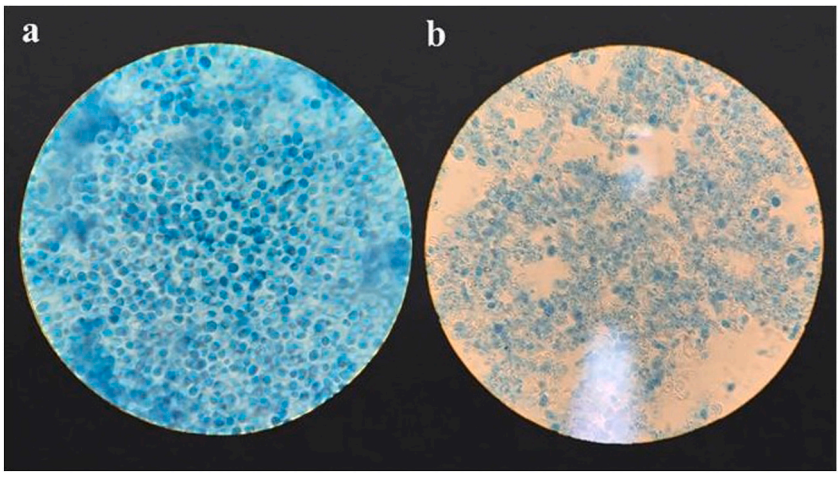

Fig. 2. The yeast cells were stained with methylene blue both a) before and, b) after the enzymatic digestion. (For interpretation of the references to color in this figure legend, the reader is referred to the Web version of this article.)

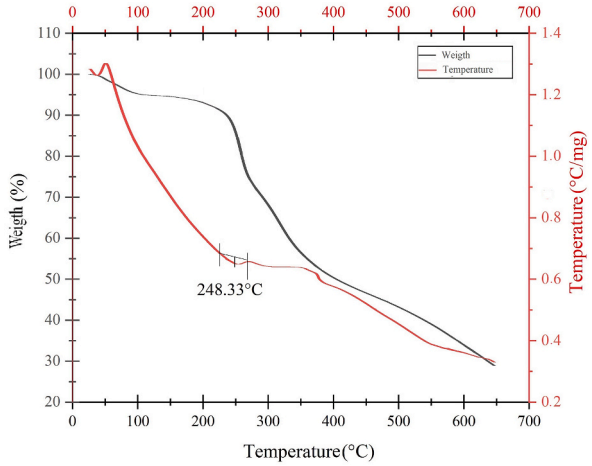

Fig. 3. TGA/DTA analysis of yeast cell wall. The phase transformation and weight loss occur at 248.33 °C.

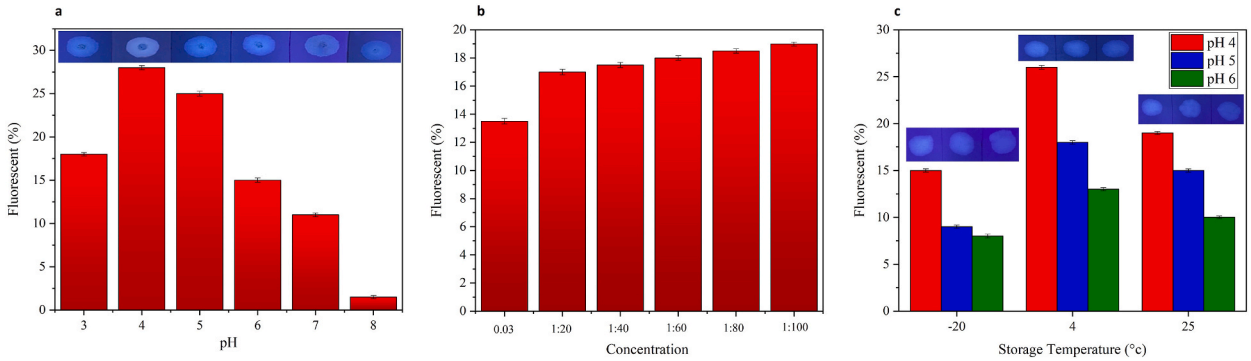

Fig. 4. Optimized condition of P-CQDs. a) Fluorescence intensity of P-CQDs at different pHs; pH 4 had the most fluorescence brightness and was chosen as the optimal pH. b) Diluting the P-CQDs solution up to 1:100 (in the optimized pH); dilution of 1:100 was chosen as the optimal diluting ratio. c) Storing of P-CQDs at different temperatures (in the optimized pH); 4 °C was chosen as the optimal storage temperature. The error bars show SD of three tests.

3.3. P-CQDs characterization

3.3.1. Optical characterization

The UV/Visible absorption spectrum of P-CQDs in the range of 190–800 nm indicated the maximum absorption at 210 nm (Fig. 5a), which is attributed to the π-π* electronic transitions of aromatic C=C bonds in the P-CQD core structure. These carbon domains give rise to the observed absorbance peak based on their characteristic electronic transitions [1,2]. Based on the photoluminescence (PL) emission spectra obtained across pH 4 to 7, 360 nm was determined to be the optimal excitation wavelength for the P-CQDs, yielding the highest emission intensity at 450 nm (Fig. 5b). This optimal excitation corresponds to the absorbance tail in the UV region and results in blue luminescence emission, demonstrating the quantum confinement effects of the synthesized P-CQDs. The blue-shifted PL peak is attributed to the quantum confinement of excitons within the nanoscale CQDs, which causes discretization of energy levels and blue-shifting of optical bandgap as the particle size approaches the exciton Bohr radius. The tunable emission spanning the visible spectrum similarly arises from quantum confinement effects that depend on CQDs size.

3.3.2. Compositional characterization

The FTIR spectra of the yeast cell wall precursor (Fig. 6a) display several dominant peaks corresponding to O–H, C–H, N–O, C=C, and C–O–C bonds. This indicates the heterogeneous, multifaceted composition of yeast cell walls, which contain diverse carbohydrates, proteins, and lipids. The variety of functional groups allows broad absorption of infrared irradiation due to the range of vibrational modes. In contrast, the P-CQDs show fewer, narrower peaks, suggesting a more homogeneous structure compared to the complex native cell wall composition. The near complete disappearance of aliphatic C–H peaks indicates the hydrocarbon components have been removed during the carbonization process, resulting in dot cores composed primarily of carbon atoms. The presence of aromatic C=C stretches (960-980 cm-1 and 1610 cm-1) confirms the P-CQD sample contains a higher fraction of conjugated sp2 carbon domains compared to the original biomass.

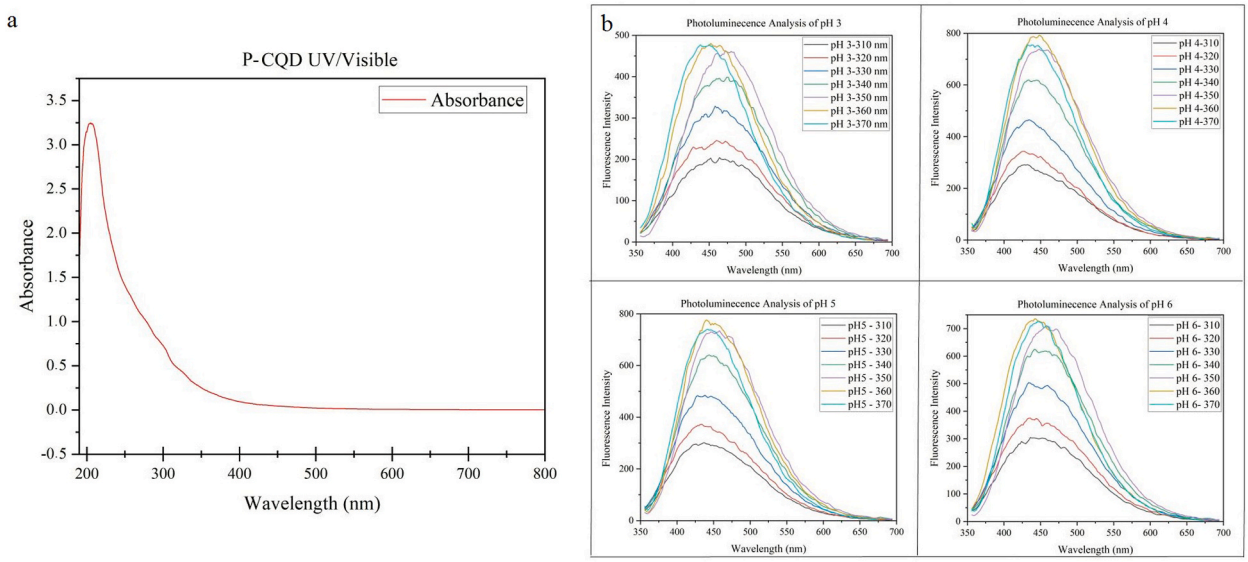

Fig. 5. Optical characterization of P-CQDs. a) UV/Visible analysis of P-CQDs. The maximum absorption was measured at 210 nm. b) PL analysis of P-CQDs at pH 3–6. The maximum excitation wavelength was obtained at 360 nm, which led to the highest emission at 450 nm. The maximum PL was detected at pH 4.

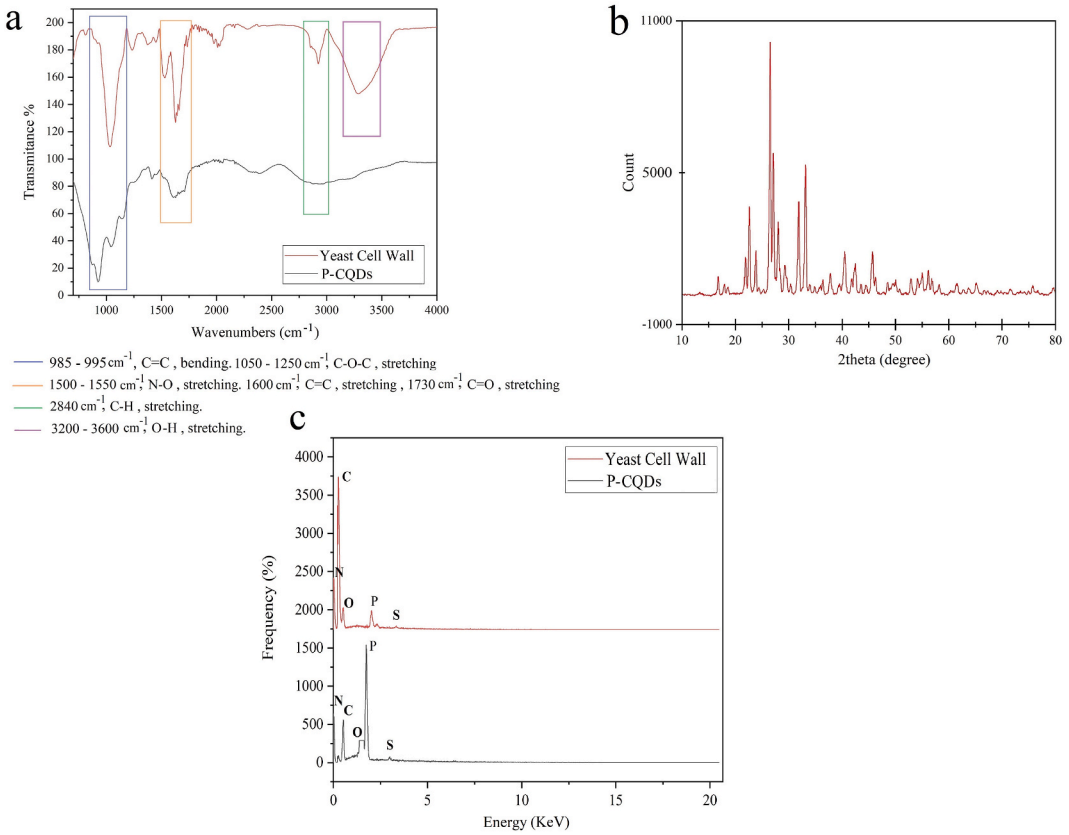

Fig. 6. Compositional characterization of P-CQDs. a) IR spectrum of mentioned yeast cell wall and P-CQDs in the frequency range of 4000-400 cm^{-1}. b) The crystalline structure of P-CQDs analyzed using XRD. c) comparison forming elements of the yeast cell wall (YCW) substrate and the P-CQDs.

Fig. 6b shows the XRD diagram of the P-CQDs following synthesis, which displays the distinctive P-CQDs peaks at 2θ equal to 21–24, 25–30, and 31–34°. The peak of 20–22° represents C=C aromatic bonds, which are compatible with the peaks identified in the FTIR. The different peaks seen in the crystal structure of P-CQDs are caused by the simultaneous presence of numerous nanostructures in it.

The EDX analysis in Fig. 6c compares the forming elements of the yeast cell wall substrate and the P-CQDs. Relative to the precursor, the P-CQDs showed a notable increase in oxygen and phosphorus content, accompanied by a decrease in carbon percentage. The heightened oxygen levels indicate the formation of additional oxygen-containing functional groups on the P-CQD surface during synthesis. More significantly, the marked increase in phosphorus confirms the successful doping of phosphate atoms within the nanocarbon core structure. This provides direct evidence for P-doping through incorporation of phosphorus hetero-atoms during carbonization of the yeast cell walls into quantum dots.

According to the results of CHNS analysis, the percentage of each element including carbon, nitrogen, hydrogen, and sulfur can be seen in the graphs related to the yeast cell wall and P-CQDs in Fig. 7a, b. The results show a prominent reduction of carbon after the synthesis of P-CQDs

3.3.3. Morphological characterization

DLS analysis indicated a uniform size distribution of nanoparticles in P-CQDs solution with a mean diameter of 3.2 ± 0.3 nm (Fig. 8a). The zeta potential of P-CQDs has measured −1.4 mV (Fig. 8b) which indicates the slightly negative charge of P-CQDs surface. The results of TEM and histogram of nanoparticle diameter dispersion are shown in Fig. 8c and d; the most distributed nanoparticles are measured in diameters of 5–7 nm.

3.3.4. Fluorescence quenching assay

In Fig. 9a, the fluorescence emission of the P-CQDs solution was tested against six different ions, including $MgSO_4$, $MnCl_2$, $ZnCl_2$, NaCl, $FeSO_4$, and $FeCl_3$. The results showed that $FeCl_3$ and to a lesser extent $FeSO_4$ quenched the fluorescence emission of P-CQDs solution. Further analysis of $FeCl_3$ showed that it can quench the synthesized P-CQDs fluorescent in a dose-dependent manner (Fig. 9b). The standard curve was plotted for 12 concentrations of $FeCl_3$ at an excitation wavelength of 360 nm (Fig. S2), and the LOD and LOQ of $FeCl_3$ were calculated to be 201 nM and 611 nM, respectively. The results of measuring Fe^{3+} in the serum sample showed a narrow range of detectable Fe^{3+} concentration (0.1–0.5 μM). Higher concentrations of Fe^{3+} did not quench the P-CQDs in a logical trend. The standard curve was drawn for the 0.1–0.5 μM range of Fe^{3+} (Fig. S3), and the LOD and LOQ were calculated to be 117.9 and 357.5 nm, respectively, in the serum sample. Since the normal range of free, or non-transferrin-bound Fe^{3+} in plasma samples is 0.6–1.3 μM [26], the synthesized P-CQDs may be applicable for the detection of free Fe^{3+} in human serum samples.

3.4. Antimicrobial, photocatalytic, and antioxidant activity

The agar well diffusion assay results showed that different concentrations of P-CQDs generated an inhibition zone in both *E. coli* and

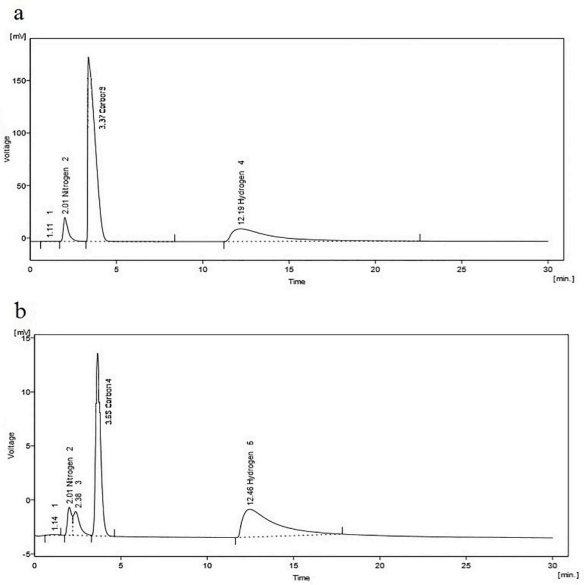

Fig. 7. Compositional characterization of YCW and P-CQDs with CHNS analysis. a) The percentage of each carbon, nitrogen, hydrogen, and sulfur element in YCW. b) The percentage of each carbon, nitrogen, hydrogen, and sulfur element in P-CQDs and a significant reduction of the carbon element.

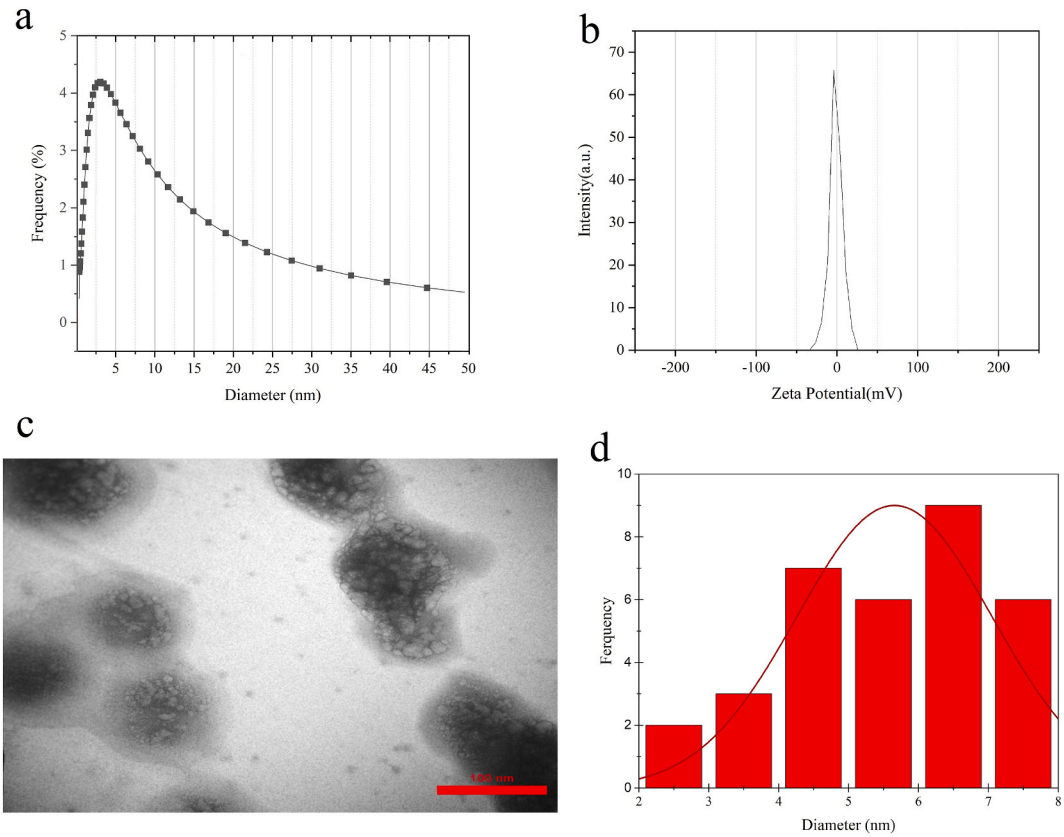

Fig. 8. Characterization of P-CQDs diameters. a) size distribution of nanoparticles in P-CQDs solution. b) Surface charge of nanoparticles in P-CQDs solution. c) TEM photo of the P-CQDs nanoparticles. d) histogram of nanoparticles diameters dispersion.

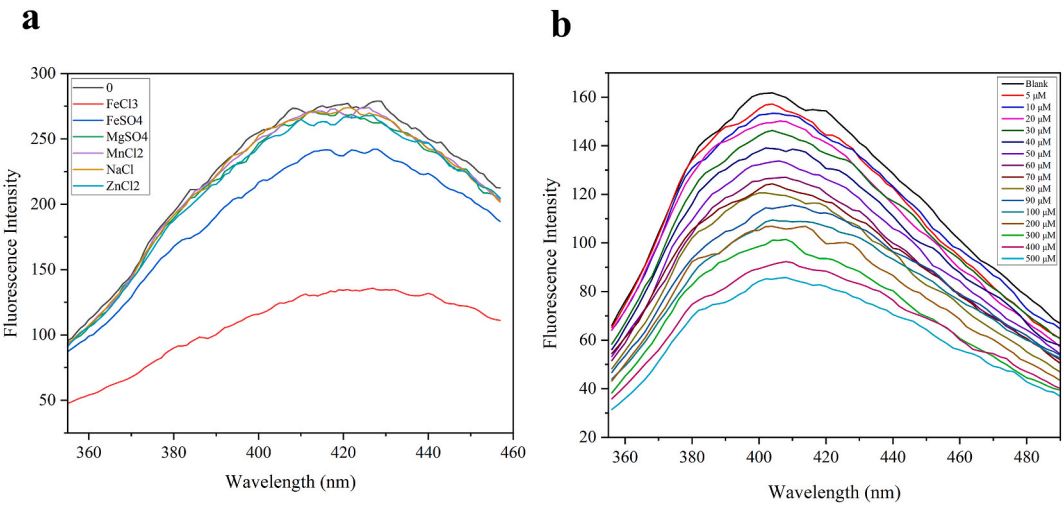

Fig. 9. a) The fluorescent quenching of 0.06 % P-CQDs solution in the presence of 0.5 mM of $MgSO_4$, $MnCl_2$, $ZnCl_2$, NaCl, $FeSO_4$, and $FeCl_3$. $FeCl_3$ significantly, and $FeSO_4$ to a lesser extent, quenched the fluorescence emission. b) Effect of different concentrations of FeCl3 on P-CQDs fluorescent quenching.

S. aureus culture plates, while the inhibition zone in the *S. aureus* culture plate was bigger (Fig. 10a and b). Fig. 10c compares the diameter of the inhibitory zones for various P-CQDs concentrations. In *E. coli* and *S. aureus* culture plates, the undiluted P-CQDs (made from a 3 % concentration of yeast cell wall) produced the greatest inhibitory zone with 2.5 times the effectiveness against *S. aureus*. P-CQDs could be diluted up to 1:100 without losing the ability to prevent the growth of *S. aureus*, however, at 1:60 there was no longer

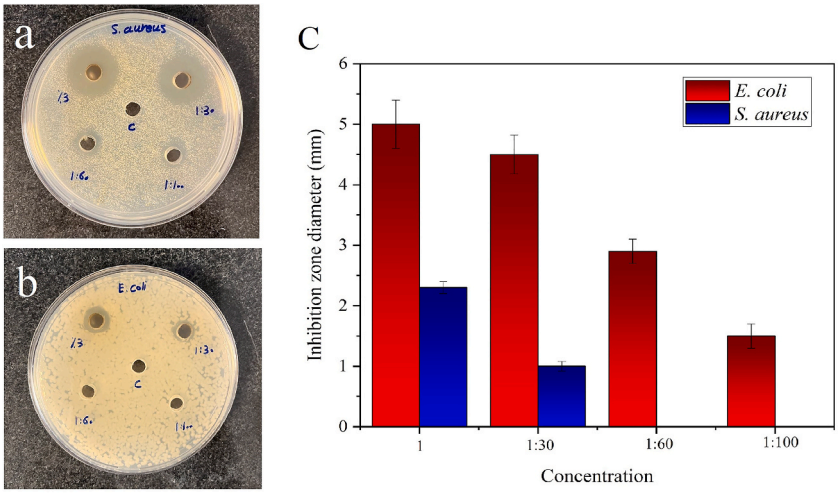

Fig. 10. Antibacterial activity of four concentrations of P-CQDs against a) *S. aureus*, b) *E. Coli*, and c) inhibition zone diameter. The error bars show the SD of three antibacterial tests on plates.

any inhibitory impact on *E. coli*.

The results of MIC and MBC, shown in Table 1, confirmed the higher antibacterial activity of synthesized P-CQDs against the gram-positive *S. aureus* than gram-negative *E. Coli*.

According to Fig. 11, the synthesized P-CQDs have significant photocatalytic activity and the concentration (value of absorbance at 662 nm) of methylene blue was decreased in the presence of P-CQDs and under sunlight irritation. The downward trend related to the photodegradation of methylene blue began after 40 min and was continued until the end of test time (200 min). The control sample incubated at the same condition, but in the dark, showed no differences in the absorbance.

Six concentrations of the Trolox standard (0, 0.1, 0.2, 0.3, 0.4, 0.5 mM) were used to prepare the standard curve (Fig. S4). The TAC of P-CQDs was calculated 2.5 mM Fe^{2+}/mg by using the obtained equation from the standard curve.

4. Discussion

CQDs are a new class of material that has emerged as a promising alternative to traditional inorganic quantum dots for sensing, medical, and imaging applications. Green synthesis of CQDs (and other nanoparticles) has gained significant attention due to several advantages including: I) using low-cost and non-toxic raw materials, which makes it an economical and eco-friendly approach [27], II) using renewable resources, which can help in reducing environmental problems such as converting agro-waste into valuable products [28], III) being a simple and facile synthesis method that does not require complex operations [29], IV) production of stable CQDs with high fluorescence, which have potential applications in various fields [30], and V) avoiding the production of CQDs from harmful and costly resources like metals, which makes it a safer and sustainable approach [28]. One of the most commonly used dopants for CQDs is phosphorous. Phosphorus doping of CQDs enhances their properties by altering the electronic state levels and producing more emissive sites in CQDs, which generates more intense fluorescence [31]. Furthermore, P-CQDs have been found to have intrinsic peroxidase activity in a wide range of pH, as well as effective antibacterial activity against *Escherichia coli* and *Staphylococcus aureus.* They can easily be made by hydrothermally treating the main precursor material and phosphoric acid [32,33]. One significant advantage of the CQDs produced from waste yeast cell walls is their low toxicity. The biocompatible carbon core derived from cell walls ensures that these nanomaterials are safer for both human health and the environment. This is a notable advantage over conventional metal-based quantum dots that contain toxic elements like cadmium [34]. Additionally, the mild hydrothermal synthesis method occurs in water using relatively benign reagents like aqueous phosphoric acid [35]. This avoids the use of hazardous organic solvents, minimizing harm to workers and the environment during production. In recent years, various green synthesis methods have been developed using natural sources such as plant extracts and food waste to produce CQDs with strong fluorescence and sharp emission peaks [27,36]. This groundbreaking study uniquely utilizes the yeast cell wall as a novel, sustainable carbon source for the environmentally friendly synthesis of P-CQDs with immense potential for biological activities. The renewability, low toxicity, and efficient use of waste biomass make this an attractive green chemistry approach to P-CQD production.

Table 1
MIC and MBC values of synthesized P-CQDsagainst *S. aureus* and *E. coli*.

MIC (μg/mL)		MBC (μg/mL)	
S. aureus	*E. coli*	*S. aureus*	*E. coli*
1.78	**7.50**	**3.75**	7.50

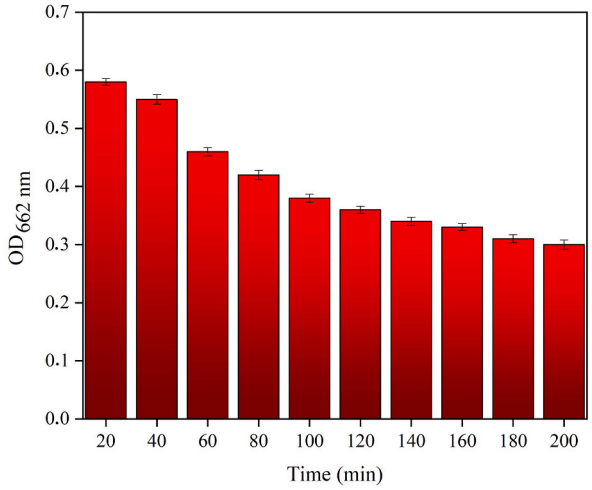

Fig. 11. The pattern of photocatalytic degradation of methylene blue by P-CQDs. The reported fluorescences represent the mean of two repeated measurements. The error bars show SD of three tests. (For interpretation of the references to color in this figure legend, the reader is referred to the Web version of this article.)

The cell wall of the yeast *Saccharomyces cerevisiae*, a by-product of yeast extract production, possesses unique properties that make it suitable for the green and sustainable synthesis of CQDs. The glucans and mannans composing the cell wall provide an abundant carbon source [37]. The reducing sugars in the mannoproteins can react during hydrothermal carbonization to form CQDs. The fibrous cell wall structure offers a high surface area for these reactions. Hydroxyl, carbonyl, and carboxyl groups on the cell walls can passivate and functionalize the CQD surfaces. The cell wall, like many other natural carbon sources, contains non-carbon atoms such as phosphorus, nitrogen, and sulfur, which can lead to the formation of CQDs with heteroatom doping and functional groups, making cell walls a promising candidate for synthesizing CQDs with exceptional bioactivity [13,38,39]. Because yeast *Saccharomyces cerevisiae* is non-toxic, the resulting CQDs have higher biocompatibility versus those from harsh chemicals. As a rapidly growing microbe that can be cultivated sustainably, *Saccharomyces cerevisiae* provides a renewable cell wall source material. Using this waste material as the precursor implements green chemistry and circular economy principles [40]. The yeast cell walls underwent enzymatic hydrolysis to extract them, leaving behind the soluble intracellular fraction. The thermal analysis determined 250 °C as the optimal temperature for hydrothermal synthesis of the CQDs. The process yielded fluorescent CQDs with a quantum yield of 19 %. The quantum yield measures the fluorescence efficiency of the photochemical synthesis process [41], and can be influenced by various factors, including the synthesis method, surface functional groups, size, and shape of the CQDs [42]. A quantum yield of 19 % is considered to be a moderate quantum yield [43]. Moderate quantum yield compounds are still considered quite fluorescent, making them useful in various applications such as imaging and sensing [43]. However, since a reaction with a higher quantum yield is more efficient, this factor serves as a benchmark for optimizing the efficiency of a reaction. Therefore, in the following studies related to these newly developed P-CQDs, we will focus on improving the quantum yield of the reaction to enhance its efficiency. After synthesis, the liquid color turns dark brown, which is an indicator of carbon-based structure formation. The synthesized P-CQDs emit slight fluorescence under UV-light irradiation which was influenced by the pH of the environment and considerably increased at pH 4 and when diluted at 1:100. Quantum dots exhibit a characteristic excitation spectrum, with a peak excitation wavelength that efficiently generates fluorescence. The excitation wavelength needs to be absorbed by the quantum dot in order to excite electrons and generate fluorescence. In the case of the present synthesized P-CQDs, a maximum excitation wavelength of 360 nm led to the highest emission at 450 nm. The excitation and emission properties of quantum dots are of particular interest for the development of advanced optoelectronic devices and sensing technologies [44]. The emitted fluorescence intensity of CQDs is affected by the protonation/deprotonation of surface chemical groups. At low pH, there is an abundance of H^+ ions that can protonate chemical groups like amines and thiols on the CQDs surface. Protonation neutralizes the surface charge of the CQDs and reduces the repulsion between particles. This causes aggregation of the CQDs, which leads to quenching of the fluorescence. At high pH, surface groups are deprotonated and negatively charged. This enhances repulsion between CQDs, minimizing aggregation and increasing fluorescence intensity. There is typically an optimal pH range, often slightly acidic (as we found in the present study), where the fluorescence intensity of CQDs is maximized due to minimized aggregation [45]. The exact optimal pH and degree of intensity change depends on the specific CQD core/shell material and surface chemistry. But in general, there is a strong dependence of CQD fluorescence on the solution pH. The pH-dependent behavior of CQDs is a valuable characteristic that could be used in controlling their optical properties, or in designing pH sensors and probes. For instance, Ji et al. used the pH-dependent photoluminescence quenching of QDs to investigate its conjugation with dopamine [46]. Optimizing the storage temperature and concentration of CQD solutions is necessary to ensure their long-term stability and maximal fluorescence intensity for downstream applications. CQD stability can be significantly impacted by storage conditions due to effects on degradation pathways and particle aggregation. In this work, we systematically evaluated the fluorescence intensity of synthesized P-CQDs stored at different temperatures and dilutions over time. Storage at 4 °C with optimized pH yielded the highest long-term fluorescence

intensity, likely due to suppressed oxidation and deformations at this temperature. Additionally, diluting the P-CQDs up to 1:100 led to markedly increased fluorescence, consistent with some previous observations. The mechanism is not fully elucidated but may arise from decreased aggregation and self-quenching at higher dilutions [42].

The compositional analysis suggests that P-CQDs have a more consistent and well-defined structure than yeast cell wall powder, with a higher concentration of aromatic bonds and increased amounts of oxygen and phosphorus. The carbonization process during hydrothermal synthesis resulted in the reduction of carbon content while increasing the amounts of oxygen and phosphorus, indicating the successful doping of CQDs with phosphorus. Identification of P-CQDs characteristics may help to understand their potential applications in biomedicine and biotechnology. For instance, the increased concentration of aromatic bonds and oxygen and phosphorus in P-CQDs may enhance their antibacterial activity, fluorescence intensity, and glucose uptake, among other potential applications [47–49]. The zeta potential measurement of −1.4 mV reveals that the P-CQDs have a slightly negative surface charge. The negative surface charge, though small, may help promote colloidal stability through electrostatic repulsion between particles. The TEM size distribution histogram shows that the most abundant particle diameters were in the 5–7 nm range, which aligns reasonably well with the average 3.2 nm diameter from DLS.

A key finding of this study was the P-CQDs' ability to detect iron ions, with significant quenching in response to Fe^{3+} and in a dose-dependent manner. Upon the addition of $FeCl_3$, it is likely that there ensues an interaction between Fe^{3+} and the surface of P-CQDs, resulting in the formation of a chelate complex between these constituents. Consequently, this complexation process may instigate static quenching, which leads to a decrease in the intrinsic luminescence of P-CQDs owing to the generation of a non-emissive species. Moreover, the presence of Fe^{3+} holds the potential to disrupt the fluorescence emission of P-CQDs through one of two mechanisms: either via inner filter effects involving reabsorption of photons or by photo-induced electron transfer processes that alter the excited state electronic configuration and cause fluorescence suppression through non-radiative pathways. Further binding studies are required to elucidate the quenching mechanism and enhance P-CQDs as fluorescent probes for Fe3+ detection [50,51]. When phosphorus is doped onto CQDs, it introduces additional functional groups on the surface of the CQDs that can interact with Fe^{3+} ions more effectively [31]. Kalaiyarasan et al. indicated that the doping of phosphorus on CQDs greatly improves the sensitivity of Fe^{3+} detection, and the quenching process is attributed to the static quenching effect, due to the formation of the fluorescently inactive P-CQDs–Fe^{3+} complex [31]. We did not see any significant differences in fluorescence for the metal ions, with the exception of Fe^{3+} and to a lesser extent Fe^{2+} ions. The quenching effect of Fe^{3+} was verified up to 500 μM of Fe^{3+} concentration and, with a LOD and LOQ of 201 and 611 nM, respectively, which ascribed to a strong affinity of P-CQDs toward Fe^{3+} than other metal ions. The low detection limit highlights the high sensitivity of synthesized P-CQDs for Fe^{3+} sensing. Fluorescent sensing of metal ions is an interesting method due to its simplicity, sensitivity, and possibility of rapid and real-time monitoring [52]. Detecting Fe3+ is critical for evaluating water quality and diagnosing diseases such as anemia, heart failure, and cancer. Iron, particularly Fe3+, plays essential roles in oxygen metabolism, electron transport, and enzymatic reactions within biological systems. However, excess or deficient levels of Fe3+ can lead to serious health problems [53,54]. So, the detection of Fe^{3+} ions is important for various applications, including biological, environmental, industrial, and material sciences [55]. For instance, the detection of Fe^{3+} ions in water can help identify sources of contamination and prevent the spread of pollutants [54]. In another study, P and N co-doped CQDs were prepared for the highly selective detection of Fe^{3+} ions and lysosomal tracking in living cells and suggested as a promising tool for cytology [56]. Here, we evaluate the potential of Fe^{3+} sensing in a biological matrix (serum), by spiking varying concentrations (0.1–1 μM) of Fe^{3+} into the diluted serum samples. Serum contains a complex milieu of proteins, cells, metabolites, and other components that can interfere and affect selectivity. Assessing performance in serum is important as the measurement of Fe^{3+} status in blood has clear clinical diagnostic relevance and reflects potential real-world application of the sensor [53]. The 0.5 μM Fe^{3+} concentration was the highest which resulted in quenching of the P-CQDs fluorescence, with the LOD and LOQ determined to be 117.9 and 357.5 nm, respectively, and high percent of the recovery. This higher sensitivity of detection for P-CQDs in serum matrix may be attributed to the positive effects of serum proteins on the dispersion and stabilization of nanoparticles, which in turn increase iron access for detection [57]. The higher Fe^{3+} concentrations did not exhibit a regular trend of further quenching, which may be due to the interference of serum components with P-CQDs and Fe^{3+} interaction at higher Fe^{3+} levels that limit further quenching.

Remarkably, the P-CQDs exhibited antimicrobial properties, with higher effectiveness against the gram-positive bacterium *S. aureus* than the gram-negative *E. coli*. The minimum inhibitory and bactericidal concentrations quantified this effect. CQDs exhibit antibacterial properties through multiple mechanisms and are influenced by factors such as size, shape, surface functional groups, and charge. Positively charged CQDs have been shown to exhibit stronger antibacterial effects due to their ability to bind more tightly to negatively charged bacterial cell walls, causing membrane disruption and cell death. However, the antibacterial activity of CQDs is not solely dependent on their surface charge, and negatively charged CQDs can still demonstrate antibacterial effects through alternative mechanisms such as the induction of oxidative stress and reactive oxygen species (ROS) production, which can damage bacterial cell walls, DNA, and other macromolecules, leading to cell death. Incorporation of hetero-atoms, such as nitrogen and phosphorous into CQDs, can enhance the generation of ROS due to the extra free electrons that they introduce into the CQDs [32,58,59]. In this study, the process of synthesizing P-CQDs involved using cell wall precursors that, as mentioned before, contain hetero-atoms such as nitrogen, sulfur, and phosphate, and the process involved an additional treatment with phosphoric acid. We found that the resulting P-CQDs had a slightly negative charge and exhibited antibacterial properties that may attributed to their ROS production capability. The antimicrobial activity of P-CQDs, along with their good biocompatibility, enhances their utility in various fields, including healthcare and food safety [60,61]. Additional promising applications of synthesized P-CQDs were demonstrated through the photodegradation of methylene blue dye by the P-CQDs under sunlight irradiation. The results showed that P-CQDs efficiently catalyzed the degradation of methylene blue over time and ~50 % of methylene blue was degraded within 200 min. This considerable photocatalytic performance of P-CQDs is attributed to the separation of photogenerated charge and suppressed electron-hole recombination, which makes them a

valuable candidate in the removal of harmful substances from the environment [62].

One of the most exciting characteristics of CQDs is their antioxidant activity, which has been extensively studied and applied in various fields. The measured TAC of P-CQDs (2.5 mM Fe^{2+}/mg) suggested a high capacity for scavenging free radicals and protecting against oxidative stress. The activity in the FRAP test may result from both antioxidant properties and the chelating effect of Fe^{3+} ions. As was discussed former, Fe^{3+} efficiently quenched the P-CQDs fluorescence, ascribed to its strong affinity toward Fe^{3+}. Iron is a transition metal that can participate in oxidation-reduction reactions, catalyzing the production of free radicals. Accumulation can promote oxidative damage. Chelating agents can bind and sequester free Fe^{3+} ions, preventing them from participating in oxidative reactions. So, by chelating Fe^{3+}, compounds can inhibit free radical formation and exhibit antioxidant effects. This is a key mechanism behind their antioxidant properties. The antioxidant capacity of P-CQDs plays a significant role in their potential biomedical applications, such as drug delivery, cell labeling and long-term bioimaging, where ROS generation can negatively affect cellular processes [63].

Overall, the results of this work lay the foundation for the development of innovative and eco-friendly nanomaterial with diverse biological activities; however, more research is needed to fully realize the potential of P-CQDs and implement them in real-world applications.

5. Conclusion

In conclusion, this manuscript provides a comprehensive study on the green synthesis of yeast cell wall-derived P-CQDs with multiple biological activities. The utilization of yeast cell walls as a carbon source for CQD synthesis presents a promising approach for sustainable nanomaterial production. The biological activities demonstrated by the P-CQDs, such as fluorescence quenching, antibacterial, photocatalytic, and antioxidant properties, open up a wide range of potential applications in various fields of science and technology. The manuscript makes a significant contribution in developing and characterizing this novel nanomaterial from an unexpected yet ideal precursor, however; further studies are warranted to explore the full potential of P-CQDs and their practical applications in real-world scenarios.

Data availability statement

No data was used for the research described in the article.

CRediT authorship contribution statement

Pardis Sadat Mirseyed: Methodology, Formal analysis, Data curation. **Sareh Arjmand:** Writing – review & editing, Writing – original draft, Validation, Supervision, Methodology, Investigation, Formal analysis, Conceptualization. **Moones Rahmandoust:** Validation, Supervision, Formal analysis. **Shahpour Kheirabadi:** Methodology. **Rojin Anbarteh:** Methodology.

Declaration of generative AI and AI-assisted technologies in the writing process

During the preparation of this work, the authors used Claudi.ai in order to improve the readability and language. After using this tool, the authors reviewed and edited the content as needed and take full responsibility for the content of the publication.

Declaration of competing interest

The authors declare that they have no known competing financial interests or personal relationships that could have appeared to influence the work reported in this paper.

Acknowledgment

The authors would like to express their gratitude to Dr. Sefidbakht for his valuable assistance and to Dr. Sara Minaeian for generously providing the bacterial strains used in this study.

This work was supported by Shahid Beheshti University, research grant. NO. 600/1898.

Appendix A. Supplementary data

Supplementary data to this article can be found online at https://doi.org/10.1016/j.heliyon.2024.e29440.

References

[1] W.C. Chan, D.J. Maxwell, X. Gao, R.E. Bailey, M. Han, S. Nie, Luminescent quantum dots for multiplexed biological detection and imaging, Curr. Opin. Biotechnol. 13 (1) (2002) 40–46.

[2] H.R. Rajabi, Photocatalytic activity of quantum dots, Semiconductor Photocatalysis-Materials, Mechanisms and Applications. 17 (2016).
[3] H. Li, Z. Kang, Y. Liu, S.-T. Lee, Carbon nanodots: synthesis, properties and applications, J. Mater. Chem. 22 (46) (2012) 24230–24253.
[4] X. Wang, P. Yang, Q. Feng, T. Meng, J. Wei, C. Xu, J. Han, Green preparation of fluorescent carbon quantum dots from cyanobacteria for biological imaging, Polymers 11 (4) (2019) 616.
[5] M.K.A. Kolaprath, L. Benny, A. Varghese, A facile, green synthesis of carbon quantum dots from Polyalthia longifolia and its application for the selective detection of cadmium, Dyes Pigments 210 (2023) 111048.
[6] S.Y. Lim, W. Shen, Z. Gao, Carbon quantum dots and their applications, Chem. Soc. Rev. 44 (1) (2015) 362–381.
[7] A. Kim, J.K. Dash, P. Kumar, R. Patel, Carbon-based quantum dots for photovoltaic devices: a review, ACS Appl. Electron. Mater. 4 (1) (2021) 27–58.
[8] A.S. Rasal, S. Yadav, A. Yadav, A.A. Kashale, S.T. Manjunatha, A. Altaee, J.-Y. Chang, Carbon quantum dots for energy applications: a review, ACS Appl. Nano Mater. 4 (7) (2021) 6515–6541.
[9] S. Kanungo, N. Gupta, R. Rawat, B. Jain, A. Solanki, A. Panday, P. Das, S. Ganguly, Doped carbon quantum dots reinforced hydrogels for sustained delivery of molecular cargo, J. Funct. Biomater. 14 (3) (2023) 166.
[10] N. Xu, S. Gao, C. Xu, Y. Fang, L. Xu, W. Zhang, Carbon quantum dots derived from waste acorn cups and its application as an ultraviolet absorbent for polyvinyl alcohol film, Appl. Surf. Sci. 556 (2021) 149774.
[11] L. Lin, Y. Luo, P. Tsai, J. Wang, X. Chen, Metal ions doped carbon quantum dots: synthesis, physicochemical properties, and their applications, TrAC, Trends Anal. Chem. 103 (2018) 87–101.
[12] S. Dinç, M. Kara, Synthesis and applications of carbon dots from food and natural products, Journal of Apitherapy and Nature 1 (1) (2018) 33–37.
[13] Y. Wu, C. Li, H.C. van der Mei, H.J. Busscher, Y. Ren, Carbon quantum dots derived from different carbon sources for antibacterial applications, Antibiotics 10 (6) (2021) 623.
[14] L.H. Nguyen, V.G. Gomes, High efficiency supercapacitor derived from biomass based carbon dots and reduced graphene oxide composite, J. Electroanal. Chem. 832 (2019) 87–96.
[15] D.E. Levin, Cell wall integrity signaling in Saccharomyces cerevisiae, Microbiol. Mol. Biol. Rev. 69 (2) (2005) 262–291.
[16] P.N. Lipke, R. Ovalle, Cell wall architecture in yeast: new structure and new challenges, J. Bacteriol. 180 (15) (1998) 3735–3740.
[17] G. Coradello, N. Tirelli, Yeast cells in microencapsulation. General features and controlling factors of the encapsulation process, Molecules 26 (11) (2021) 3123.
[18] C. Camara, Clinical trials involving children and young people, Br. J. Nurs. 28 (21) (2019) 1370–1373.
[19] P. Orlean, Biogenesis of yeast wall and surface components, Cell cycle and cell, biology 21 (1997) 229–362.
[20] S.O. Asare, Optimized Acid/base Extraction and Structural Characterization of β-glucan from Saccharomyces cerevisiae, East Tennessee State University, 2015.
[21] A. Vassilakopoulou, V. Georgakilas, N. Vainos, I. Koutselas, Successful entrapment of carbon dots within flexible free-standing transparent mesoporous organic-inorganic silica hybrid films for photonic applications, J. Phys. Chem. Solid. 103 (2017) 190–196.
[22] B. Shi, Y. Su, L. Zhang, M. Huang, R. Liu, S. Zhao, Nitrogen and phosphorus co-doped carbon nanodots as a novel fluorescent probe for highly sensitive detection of Fe3+ in human serum and living cells, ACS Appl. Mater. Interfaces 8 (17) (2016) 10717–10725.
[23] M. Balouiri, M. Sadiki, S.K. Ibnsouda, Methods for in vitro evaluating antimicrobial activity: a review, Journal of pharmaceutical analysis 6 (2) (2016) 71–79.
[24] I. Khan, K. Saeed, I. Zekker, B. Zhang, A.H. Hendi, A. Ahmad, S. Ahmad, N. Zada, H. Ahmad, L.A. Shah, Review on methylene blue: its properties, uses, toxicity and photodegradation, Water 14 (2) (2022) 242.
[25] D. Huang, B. Ou, R.L. Prior, The chemistry behind antioxidant capacity assays, J. Agric. Food Chem. 53 (6) (2005) 1841–1856.
[26] I. Gosriwatana, O. Loreal, S. Lu, P. Brissot, J. Porter, R.C. Hider, Quantification of non-transferrin-bound iron in the presence of unsaturated transferrin, Anal. Biochem. 273 (2) (1999) 212–220.
[27] V. Manikandan, N.Y. Lee, Green synthesis of carbon quantum dots and their environmental applications, Environ. Res. 212 (2022) 113283.
[28] H.H. Jing, F. Bardakci, S. Akgöl, K. Kusat, M. Adnan, M.J. Alam, R. Gupta, S. Sahreen, Y. Chen, S.C. Gopinath, Green carbon dots: synthesis, characterization, properties and biomedical applications, J. Funct. Biomater. 14 (1) (2023) 27.
[29] J.P. Malavika, C. Shobana, S. Sundarraj, M. Ganeshbabu, P. Kumar, R.K. Selvan, Green synthesis of multifunctional carbon quantum dots: an approach in cancer theranostics, Biomater. Adv. (2022) 212756.
[30] L.J. Desmond, A.N. Phan, P. Gentile, Critical overview on the green synthesis of carbon quantum dots and their application for cancer therapy, Environ. Sci.: Nano 8 (4) (2021) 848–862.
[31] G. Kalaiyarasan, J. Joseph, P. Kumar, Phosphorus-doped carbon quantum dots as fluorometric probes for iron detection, ACS Omega 5 (35) (2020) 22278–22288.
[32] S. Chai, L. Zhou, S. Pei, Z. Zhu, B. Chen, P-doped carbon quantum dots with antibacterial activity, Micromachines 12 (9) (2021) 1116.
[33] K.M. Tripathi, H.T. Ahn, M. Chung, X.A. Le, D. Saini, A. Bhati, S.K. Sonkar, M.I. Kim, T. Kim, N, S, and P-co-doped carbon quantum dots: intrinsic peroxidase activity in a wide pH range and its antibacterial applications, ACS Biomater. Sci. Eng. 6 (10) (2020) 5527–5537.
[34] I. Singh, R. Arora, H. Dhiman, R. Pahwa, Carbon quantum dots: synthesis, characterization and biomedical applications, Turk J. Pharm. Sci. 15 (2) (2018) 219–230.
[35] B. Li, M. Berliner, R. Buzon, C.K.-F. Chiu, S.T. Colgan, T. Kaneko, N. Keene, W. Kissel, T. Le, K.R. Leeman, Aqueous phosphoric acid as a mild reagent for deprotection of tert-butyl carbamates, esters, and ethers, J. Org. Chem. 71 (24) (2006) 9045–9050.
[36] E. Dhandapani, N. Duraisamy, R.M. Raj, Green synthesis of carbon quantum dots from food waste, Mater. Today: Proc. 51 (2022) 1696–1700.
[37] S. Bartnicki-Garcia, Fungal cell wall composition, in: Handbook of Microbiology, CRC Press, 2019, pp. 483–496.
[38] S. Bindschedler, L. Millière, G. Cailleau, D. Job, E. Verrecchia, Calcitic nanofibres in soils and caves: a putative fungal contribution to carbonatogenesis, Geological Society, London, Special Publications 336 (1) (2010) 225–238.
[39] J. Bacon, Nature and disposition of polysaccharides within the cell envelope, in: Yeast Cell Envelopes Biochemistry Biophysics and Ultrastructure, CRC Press, 2018, pp. 65–84.
[40] M. Parapouli, A. Vasileiadis, A.-S. Afendra, E. Hatziloukas, Saccharomyces cerevisiae and its industrial applications, AIMS microbiology 6 (1) (2020) 1.
[41] S.C. Ortiz, E.M. Ospino, R. Cabanzo, Spectroscopy characterization and quantum yield determination of quantum dots, in: Journal of Physics: Conference Series, IOP Publishing, 2016 012097.
[42] S. Dua, P. Kumar, B. Pani, A. Kaur, M. Khanna, G. Bhatt, Stability of carbon quantum dots: a critical review, RSC Adv. 13 (20) (2023) 13845–13861.
[43] J.R. Swierk, The cost of quantum yield, Org. Process Res. Dev. 27 (7) (2023) 1411–1419.
[44] L. Sai, S. Jiao, J. Yang, Ultraviolet carbon nanodots providing a dual-mode spectral matching platform for synergistic enhancement of the fluorescent sensing, Molecules 25 (11) (2020) 2679.
[45] Y. Guo, L. Zhang, F. Cao, Y. Leng, Thermal treatment of hair for the synthesis of sustainable carbon quantum dots and the applications for sensing Hg2+, Sci. Rep. 6 (1) (2016) 35795.
[46] X. Ji, G. Palui, T. Avellini, H.B. Na, C. Yi, Jr KL. Knappenberger, H. Mattoussi, On the pH-dependent quenching of quantum dot photoluminescence by redox active dopamine, J. Am. Chem. Soc. 134 (13) (2012) 6006–6017.
[47] S. Chai, L. Zhou, Y. Chi, L. Chen, S. Pei, B. Chen, Enhanced antibacterial activity with increasing P doping ratio in CQDs, RSC Adv. 12 (43) (2022) 27709–27715.
[48] S. Zhao, X. Chen, C. Zhang, P. Zhao, A.J. Ragauskas, X. Song, Fluorescence enhancement of lignin-based carbon quantum dots by concentration-dependent and electron-donating substituent synergy and their cell imaging applications, ACS Appl. Mater. Interfaces 13 (51) (2021) 61565–61577.
[49] S. Zhao, X. Song, X. Chai, P. Zhao, H. He, Z. Liu, Green production of fluorescent carbon quantum dots based on pine wood and its application in the detection of Fe3+, J. Clean. Prod. 263 (2020) 121561.
[50] F. Liu, S. Zhu, D. Li, G. Chen, S.-H. Ho, Detecting ferric iron by microalgal residue-derived fluorescent nanosensor with an advanced kinetic model, iScience 23 (6) (2020).
[51] S. Gurung, N. Arun, M. Joshi, T. Jaiswal, A.P. Pathak, P. Das, A.K. Singh, A. Tripathi, A. Tiwari, Dual metal ion (Fe3+ and As3+) sensing and cell bioimaging using fluorescent carbon quantum dots synthesised from Cynodon dactylon, Chemosphere 339 (2023) 139638.

[52] Y. Chen, X. Sun, W. Pan, G. Yu, J. Wang, Fe3+-sensitive carbon dots for detection of Fe3+ in aqueous solution and intracellular imaging of Fe3+ inside fungal cells, Front. Chem. 7 (2020) 911.
[53] S.S. Mati, D. Singharoy, B. Samai, S. Konar, N. Santra, S. Pal, P. Das, S. Murmu, Exploring selective recognition between Fe2+, Fe3+ and their implementation in bio-imaging: a combined spectroscopic and theoretical investigation, J. Mol. Struct. 1184 (2019) 102–109.
[54] W. Ji, Z. Zhu, S. Dong, J. Nie, B. Du, Optical detection of Fe3+ ions in aqueous solution with high selectivity and sensitivity by using sulfasalazine functionalized microgels, Sensors 19 (19) (2019) 4223.
[55] S. Gao, X. Wang, N. Xu, H. Lian, L. Xu, W. Zhang, C. Xu, From coconut petiole residues to fluorescent carbon dots via a green hydrothermal method for Fe 3+ detection, Cellulose 28 (2021) 1647–1661.
[56] Y. Xing, M. Yang, X. Chen, Fabrication of P and N Co-doped carbon dots for Fe3+ detection in serum and lysosomal tracking in living cells, Biosensors 13 (2) (2023) 230.
[57] G. Bashiri, M.S. Padilla, K.L. Swingle, S.J. Shepherd, M.J. Mitchell, K. Wang, Nanoparticle protein corona: from structure and function to therapeutic targeting, Lab Chip 23 (6) (2023) 1432–1466.
[58] Q. Li, X. Shen, D. Xing, Carbon quantum dots as ROS-generator and-scavenger: a comprehensive review, Dyes Pigments 208 (2023) 110784.
[59] W. Bing, H. Sun, Z. Yan, J. Ren, X. Qu, Programmed bacteria death induced by carbon dots with different surface charge, Small 12 (34) (2016) 4713–4718.
[60] M. Ghirardello, J. Ramos-Soriano, M.C. Galan, Carbon dots as an emergent class of antimicrobial agents, Nanomaterials 11 (8) (2021) 1877.
[61] S. Pandiyan, L. Arumugam, S.P. Srirengan, R. Pitchan, P. Sevugan, K. Kannan, G. Pitchan, T.A. Hegde, V. Gandhirajan, Biocompatible carbon quantum dots derived from sugarcane industrial wastes for effective nonlinear optical behavior and antimicrobial activity applications, ACS Omega 5 (47) (2020) 30363–30372.
[62] H. Jung, V.S. Sapner, A. Adhikari, B.R. Sathe, R. Patel, Recent progress on carbon quantum dots based photocatalysis, Front. Chem. 10 (2022) 881495.
[63] Ł. Janus, J. Radwan-Pragłowska, M. Piątkowski, D. Bogdał, Smart, tunable CQDs with antioxidant properties for biomedical applications—ecofriendly synthesis and characterization, Molecules 25 (3) (2020) 736.